The Astrophysical Journal, 682:68–80, 2008 July 20

TOWARD EQUATIONS OF GALACTIC STRUCTURE

Dennis Zaritsky,[1] Ann I. Zabludoff,[1] and Anthony H. Gonzalez[2]
Received 2007 November 13; accepted 2008 January 16

ABSTRACT

We find that all classes of galaxies, ranging from disks to spheroids and from dwarf spheroidals to brightest cluster galaxies, lie on a two-dimensional surface within the space defined by the logarithms of the half-light radius, r_e, mean I-band surface brightness within r_e, I_e, and internal velocity $V^2 \equiv (1/2)v_c^2 + \sigma^2$, where v_c is the rotational velocity and σ is the velocity dispersion. If these quantities are expressed in terms of kpc, $L_\odot$ pc^{-2}, and km s^{-1}, then this surface is described by the equation $\log r_e - \log V^2 + \log I_e + \log \Upsilon_e + 0.8 = 0$, where we provide a fitting function for Υ_e, the mass-to-light ratio within r_e in units of $M_\odot/L_\odot$, that depends only on V and I_e. The scatter about this surface for our heterogeneous sample of 1925 galaxies is small (<0.1 dex), and both the scatter within one of the galaxy subsamples (1319 disks) and the analysis of subsamples with independently derived mass-to-light ratios suggest that the intrinsic scatter could be as low as ~0.05 dex, or 10%, prior to any correction for observational errors. This small scatter has three possible implications for how gross galactic structure is affected by internal factors, such as stellar orbital structure, nuclear activity, or mass loss history, and by external factors, such as environment or accretion history. These factors either (1) play no role beyond generating some of the observed scatter, (2) move galaxies along the surface, or (3) balance each other to maintain this surface as the locus of galactic structure equilibria. We cast the behavior of Υ_e in terms of the fraction of baryons converted to stars, η, and the concentration of those stars within the dark matter halo, $\xi \equiv R_{200}/r_e$, where R_{200} is the standard estimate of the virial radius. We derive expressions for η and ξ, use an independent measurement of η to evaluate leading constant terms, obtain $\eta = 1.9 \times 10^{-5}(L/L^*)\Upsilon_* V^{-3}$ and $\xi = 1.4 V r_e^{-1}$, and relate these to each other via $\log \eta + \log \xi = -\log \Upsilon_e + \log \Upsilon_* + \text{const}$. Finally, we present the distributions of η and ξ for the full range of galaxies and conclude that the high Υ_e of dSph's are due to low η, rather than any differences in ξ, that η is similar for spheroids and disks of a given V, and that η decreases with increasing V for systems with $V > 30$ km s^{-1}. For systems with internal velocities comparable to that of the Milky Way (149 km s^{-1} < V < 163 km s^{-1}), $\eta = 0.14 \pm 0.05$, and ξ is, on average, ~5 times greater for spheroids than for disks.

Subject headings: galaxies: formation — galaxies: structure

1. INTRODUCTION

Are galaxies fundamentally a simple family of collapsed objects, whose gross structure is describable by a few basic parameters, or are they highly complex systems whose structural properties are determined by a myriad of internal and external factors? If the former, there must be a construct analogous to the stellar Hertzsprung-Russell (H-R) diagram that testifies to deep, systemic structural patterns among galaxies and serves as a guide to a simple, if not entirely complete, analytic description of galactic structure. The study of stellar structure offers a beautiful example of the power of reductionism in astrophysics. By focusing on the H-R diagram, investigators solved the problem of stellar structure without needing to address other unsolved problems, such as the origin of the initial mass function. The observation that the position of main-sequence stars on the H-R diagram is insensitive to their location in the Galaxy indicates that their structure does not depend sensitively on parameters that vary from one place to another. We now know that mass is the primary determinant of where a star lies on the main sequence. Other physical characteristics, such as age, metallicity, and rotation, affect stellar colors and magnitudes (and therefore should be included in a complete model of stellar structure), but they are relatively minor factors along the main sequence and can be neglected in the interest of isolating the basic physics.

Among galaxies there are hints of analogous "sequences." These are referred to as galaxy scaling laws and include the Faber-Jackson (FJ; Faber & Jackson 1976) and Tully-Fisher relations (TF; Tully & Fisher 1977), the fundamental plane (FP; Djorgovski & Davis 1987; Dressler et al. 1987), and the fundamental manifold (FM; Zaritsky et al. 2006a, 2006b). Although it is not yet evident that any of these is as fundamental for galaxies as the main sequence is for stars, they do imply that a limited number of parameters characterize the gross properties of at least certain subsets of galaxies.

There are two arguments against using existing galaxy scaling laws as guides to a more nearly complete description of galactic structure. First, existing scaling laws work only over a limited range of galaxy types and luminosities. While this is not an insurmountable obstacle—not all stars lie on the main sequence—it suggests that the current scaling laws are incomplete and that they will not lead to a description of all galaxies. Second, for historical reasons related to the empirical nature of the scaling laws, their current formulation is not optimal with respect to possible theoretical constructs. For example, one determination of the fundamental plane has $\log r_e = 1.24 \log \sigma - 0.82 \log I_e + \gamma$ (Jørgensen et al. 1996), where r_e is the half-light radius, σ is the velocity dispersion, I_e is the surface brightness within r_e, and γ is a constant. It is unlikely that a simple theory would reproduce the 1.24 and 0.82 coefficients.

In this paper, we attempt to address both of these shortcomings. Although we are not the first to hope to identify a unifying description of galaxies (see κ-space; Burstein et al. 1997), we achieve three of our key goals: (1) to find an empirical relationship

[1] Steward Observatory, University of Arizona, 933 North Cherry Avenue, Tucson, AZ 85721; azabludoff@as.arizona.edu, azabludoff@as.arizona.edu.
[2] Department of Astronomy, University of Florida, Gainesville, FL 32611; anthony@astro.ufl.edu.

for *all* galaxies that has scatter comparable to those relations identified previously for limited subsets of galaxies (TF, FJ, FP, and FM), (2) to isolate the critical additional knowledge beyond the virial theorem that is needed to derive this relationship, and (3) to begin constructing the bridge between a purely empirical relationship that utilizes observables and a theoretical one that is based on physical parameters.

In summary, we begin from basic dynamical principles and examine the dimensionality of the family of galaxies, ranging from dSph's to brightest cluster galaxies and from disks to spheroids. We address our basic question, how uniform are the gross structural properties of galaxies?, by determining that a single scaling relation exists that spans all luminosities and galaxy types and by quantifying its scatter. We employ an extended version of the fundamental plane formalism that reproduces the structural properties of all galaxies at a level comparable to that achieved with either the TF relation for disks or the FP for spheroids. We establish that connecting this new scaling relation to the virial theorem requires knowledge only of the mass-to-light ratio within r_e and Υ_e and that Υ_e can be accurately modeled as a function of the observed structural parameters themselves. We proceed to describe Υ_e as a combination of the fraction of baryons converted into stars, η, and the degree to which those stars are packed within the dark matter halo, ξ. Using our empirical findings, we then calculate these two physical parameters for all of our galaxies and compare η with independent measurements. The aim of this work is to define simple expressions for basic physical parameters of galaxies that may illustrate which physical processes drive the observed patterns of galactic structure, with the expectation that this will focus subsequent, more detailed theoretical work.

2. THE DATA

To determine the degree to which all galaxies are structurally similar, we need structural parameter measurements for galaxies ranging from spheroids to disks and giants to dwarfs. Part of the legacy of distinct scaling relations for different classes of galaxies are studies that provide the relevant information only for those particular classes of galaxies. For example, there are extensive studies of spheroidal galaxies (e.g., Jørgensen et al. 1996) that are entirely distinct from those of spiral galaxies (e.g., Springob et al. 2007). This dichotomy is partly due to the techniques necessary to measure the internal dynamics for disks and spheroids, but it also leads to the use of different photometric systems and definitions. It is impossible to resolve all of those differences, and many existing galaxy samples cannot be included here because they lack some necessary measurements. We describe the spheroid and disk samples that we use below. These constitute a heterogeneous data set, but span the full range of galaxy types and luminosities and require minimal corrections for internal comparisons. It is a testament to the robustness of our results that the many differences among the samples that we either ignore or only crudely correct (such as correcting the photometry to *I* band on the basis of average colors for different galaxy populations) do not derail this investigation.

2.1. *Spheroids*

Since Zaritsky et al. (2006b), there has been one key improvement in the available data on low-mass spheroids. Simon & Geha (2007) present velocity dispersions and a uniform set of structural parameters for eight additional Local Group dSph's, including some of the lowest luminosity systems known. Adding these data to the Zaritsky et al. (2006a) compilation greatly increases our sample for extreme values of luminosity, internal velocity, and effective radius. The lack of such data earlier precluded our use of this range in the *fitting* of the FM, and instead we showed that an extrapolation of the FM accurately fit galaxies in this parameter range (Zaritsky et al. 2006b). Here we fit to both the previous data for the entire range of spheroid masses (Zaritsky et al. 2006a, 2006b and references therein) and the new data for low-mass spheroids (Simon & Geha 2007). These galaxies lie in a range of environments from poor groups (with a velocity dispersion, σ, of a few hundred km s^{-1}) to rich clusters ($\sigma > 1000$ km s^{-1}).

2.2. *Disks*

We focus on three particular disk samples, Pizagno et al. (2007), Springob et al. (2007), and Geha et al. (2006). Here we briefly describe the various data sets.

Of the three samples, the Pizagno et al. (2007) sample allows the simplest comparison to the spheroid samples. The authors provide half-light radii, *i*-band magnitudes, and a range of velocity measures from their optical rotation curves of a galaxy sample selected broadly in terms of mass, type, and environment. As they did for their Tully-Fisher analysis, we use their V_{80} measurement, which is a measure of the rotation velocity at a radius that encloses 80% of the galaxy light. We correct the *i*-band magnitudes to Johnson *I* by subtracting 0.4 mag (Fukugita et al. 1995).

The next simplest sample for comparison is that of Springob et al. (2007), who provide H I measurements of the rotation and *I*-band photometry of both field and cluster spiral galaxies. They do not tabulate half-light radii, so we calculate them based on the measures they do provide, the radius that encloses 83% of the light and the radius of the 23.5 mag arcsec^{-2} isophote, assuming an exponential surface brightness profile. Among galaxies for which all of the relevant data exist, we reject only systems with $cz < 2500$ km s^{-1}, to avoid the local flow field.

Finally, the Geha et al. (2006) sample is distinct because it is primarily composed of low-luminosity systems with very large gas mass fractions. Because gas fractions are low in normal spiral galaxies (Read & Trentham 2005), the gas can be ignored with little impact when studying scaling relations such as TF for such spiral galaxies. However, studies of low-mass galaxies show that accounting for all the baryons is critical in maintaining the scaling relation (McGaugh et al. 2000, 2005; Geha et al. 2006). Therefore, we discuss the Geha et al. (2006) sample separately in § 3.4. We use their inclination- and turbulence-corrected velocities and transform from *r* to *I* magnitudes using the colors of late-type spiral galaxies and the tabulations of Fukugita et al. (1995).

3. RESULTS AND DISCUSSION

3.1. *Proceeding from the Virial Theorem*

In this section, we revisit the standard derivation of the FP to provide a framework and physical intuition for our observational results. We begin with the tensor virial theorem, use simplifying assumptions to rewrite the virial theorem in terms of observed quantities where possible, discuss the resulting equation and its implications for the nature of galactic structure, and finally suggest a way to proceed, even though some terms in the resulting equation cannot be expressed in terms of observed quantities. We apply this suggestion and explore it in quantitative detail in §§ 3.2 and 3.3.

We begin with the tensor virial theorem,

$$\frac{1}{2}\frac{d^2\mathbf{I}_{jk}}{dt^2} = 2\mathbf{T}_{jk} + \Pi_{jk} + \mathbf{W}_{jk}, \quad (1)$$

where $\mathbf{T}$ and Π are the contributions to the kinetic energy tensor from the ordered and random motions, $\mathbf{W}$ is the potential energy

tensor, and **I** is the moment of inertia tensor. In steady state, the left-hand side of equation (1) is zero. We evaluate the trace of this equation and express the ordered component of the kinetic energy as $(1/2)A_0Mv_c^2$ and the random component as $A_1M\sigma^2$, where v_c is the circular velocity in disk galaxies, σ is the line-of-sight velocity dispersion for spheroidals, M is the mass of the system, and the A_n represent the correction factors obtained by fully evaluating the appropriate integrals. Similarly, the potential energy is expressed as $-B_0GM^2/R$, where R is a characteristic radius that we define to be the half-light radius, r_e, and B_0 is a correction factor obtained by fully evaluating the appropriate integral. Hence, without loss of generality,

$$A_0v_c^2 + A_1\sigma^2 = B_0\frac{GM}{r_e}. \quad (2)$$

All of the possible real-world complications are encapsulated in the yet unspecified A_n and B_0, and, in principle, these could be extremely complicated functions of the formation history and environment of galaxies. The only assumption that we have made so far is that the virial theorem holds over these radii, which is reasonable for galaxies because $r_e \ll r_{\rm vir}$.

To numerically evaluate equation (2), we now introduce two sets of simplifying assumptions that we will eventually test by determining whether we reproduce the observations. First is the kinematic simplification. We reduce the number of A parameters by requiring $A_0v_c^2 + A_1\sigma^2 \equiv AV^2$, where $V \equiv (1/2)v_c^2 + \sigma^2$. This simplification is accurate if we are dealing with isothermal spheres and isotropic velocity dispersions. In such systems, at large radii v_c for a purely rotationally supported population equals $\sqrt{2}\sigma$ for a purely pressure-supported population. Furthermore, in such a pressure-supported system, the internal velocity dispersion is equal to the line-of-sight velocity dispersion. To evaluate V for disk galaxies, we use the measured v_c and set $\sigma = 0$, while for spheroidal galaxies we use the measured σ and set $v_c = 0$.

Although the kinematic simplification relies on highly specific assumptions, both disks and spheroids satisfy the relevant conditions well, and this conversion has been used previously in various contexts (Burstein et al. 1997; Kassin et al. 2007). Optical disks are characterized by flat rotation curves, which imply that the mass profile is that of an isothermal sphere over these radii and that the velocity tracers, H II regions or neutral hydrogen, are on circular orbits (see Faber & Gallagher 1979). Spheroids also lie in mass distributions that are consistent with being isothermal spheres (Gavazzi et al. 2007), and their stellar velocity dispersions are nearly isotropic if the system is a slow rotator (Cappellari et al. 2007). Due to the nature of our spheroid samples, we expect that there are strong selection biases against fast rotators among the more luminous systems (i.e., they would often be removed from fundamental plane studies), and the lowest luminosity systems show little rotation (Walker et al. 2007). Therefore, our sample is likely to satisfy the assumptions involved in the kinematic simplification, but we discuss possible signatures of failure in § 3.5.

Continuing in our attempt to convert equation (2) into an equation that we can numerically evaluate, our second simplification involves the replacement of the difficult-to-measure M with M_e, the mass enclosed at r_e. We refer to this as the mass simplification. We rewrite M_e as Υ_eL_e so that it is expressed as a function of observable quantities, namely, L_e and Υ_e, the luminosity ($\equiv\pi r_e^2I_e$), and the mass-to-light ratio within r_e, respectively. In principle, the relationship that we derive is passband independent, unlike TF, for example, because we explicitly use the combination of Υ_e and I_e to estimate the mass enclosed within r_e. In practice, because

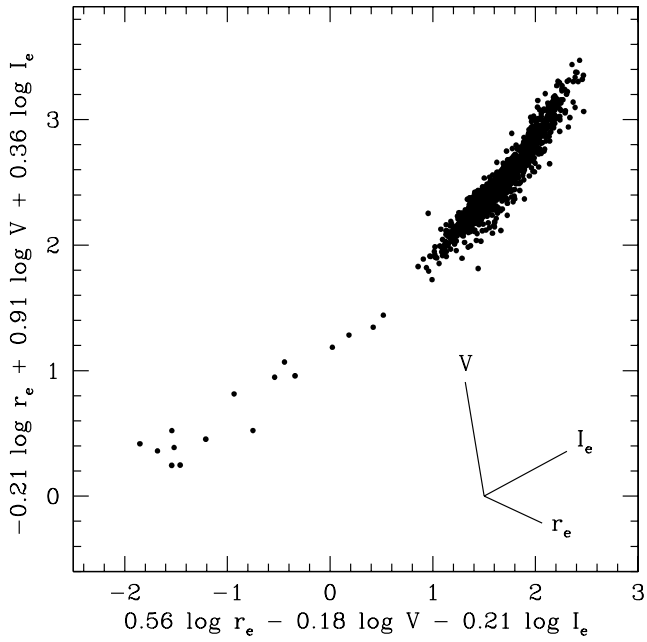

FIG. 1.—Distribution of galaxies (444 spheroids and 1481 disks) in the (r_e, I_e, V) space. This projection was chosen by eye to demonstrate that galaxies lie on a fairly well-defined surface. The data are discussed in § 2. The axes at bottom right show the orientation of the three-dimensional space. The poorly populated tail consists of Local Group dwarfs and would be, we expect, well populated in a volume-limited sample. Units for the three axes are kpc, $L_\odot$ pc^{-2}, and km s^{-1}, where $V = v_c/\sqrt{2}$ for disks and $V = \sigma$ for spheroids.

r_e is likely to be band dependent, there may be a slight band dependency in the final observed scatter and in the normalization of the final relationship. We then replace B_0 with B to account for the unknown difference between M and M_e.

We now apply the kinematic and mass simplifications to equation (2), rewriting it as

$$AV^2 = BG\pi\Upsilon_e r_e I_e. \quad (3)$$

Finally, we take the logarithm of both sides and rearrange terms to obtain

$$\log r_e - \log V^2 + \log I_e + \log \Upsilon_e - \log A + \log B = \text{const}. \quad (4)$$

This equation leads to the rather dispiriting conclusion that galaxies populate at least a six-dimensional parameter space—more if yet unspecified parameters, such as Υ_e, are actually functions of additional parameters, such as age, metallicity, formation history, bulge-to-disk ratio, or environment. Surprisingly, as shown in Figure 1, galaxies populate a limited region of the (r_e, I_e, V) space, indicating a much lower dimensionality.

One way in which the dimensionality of the galaxy family might be reduced from that suggested by equation (4) is if Υ_e, A, and B are functions *only* of r_e, I_e, and V. A simple variant of this scaling is referred to as "homology," in which the functional forms are assumed to be power laws. Because of the logarithms, the effect of rewriting equation (4) in such a variant is a change in the coefficients of the log V^2 and log I_e terms. Therefore, the assumption of homology results in a prediction that galaxies lie on a plane in the (r_e, I_e, V) space. The values of the coefficients describe the tilt of that plane. The success of the fundamental plane description for giant elliptical galaxies (Djorgovski & Davis 1987; Dressler et al. 1987; Jørgensen et al. 1996; Bernardi et al. 2003)

demonstrates that, over the limited mass range of these galaxies, the homology assumption holds surprisingly well. This success was extended in the κ-space formalism of Burstein et al. (1997), in which different classes of objects were found to lie on different planes. However, the failure of a single plane to describe the distribution of all spheroidal galaxies demonstrates that over a more extended mass range, which includes the most and least massive spheroids, homology does not hold (Zaritsky et al. 2006a).

Here we take a different approach in that we (1) assume that *all* galaxies (faint, luminous, disk, and spheroid) fall on a single manifold in the (r_e, I_e, V) space and (2) examine the behavior of Υ_e that would make that possible. This approach is motivated by our earlier finding that the behavior of Υ_e is both simple and qualitatively reasonable for all spheroids (Zaritsky et al. 2006a, 2006b), leading to what we termed the fundamental manifold (FM) of spheroids. So emboldened, we now assert that for all galaxies, deviations from homology are dominated by the behavior of Υ_e, ignoring variations in A and B among galaxies.[3] Our approach here represents a philosophical departure from ours and others' earlier work, which usually focused on establishing or quantifying the tight empirically derived scaling relationships (e.g., the FP or FM), because we posit the existence of a fundamental manifold of all galaxies and then examine the implications.

3.2. *The Simplicity of Galaxies*

The treatment described in § 3.1 and culminating in equation (4) is incomplete. The simple theoretical approach fails because it does not predict the low dimensionality of the data seen in Figure 1. On the other hand, the purely empirical treatment of fitting a manifold to the data in the (r_e, I_e, V) space fails because it does not connect the actual functional form to a physical framework. Much like the case with the FP coefficients, directly fitting the data will subsume the behavior of Υ_e, A, and B in equation (4) into the coefficients of the various structural terms (see axes in Fig. 1). Instead, we merge the two approaches by retaining the values of the coefficients derived from the virial theorem treatment as given in equation (4), assert that the most distinct break from homology occurs in Υ_e, set A and B to be constants, and then solve for Υ_e,

$$\log \Upsilon_e = \log V^2 - \log I_e - \log r_e + \text{const}. \quad (5)$$

This approach may seem like only mathematical sleight of hand, but we will quantitatively test our association of Υ_e with the dominant departures from homology in § 3.3.

To proceed, we evaluate $\log \Upsilon_e - \text{const}$ using equation (5) and plot the results in Figure 2. We then fit for the function, $\log \Upsilon_e^f$, that describes these data and also plot the calculated values using this fit in Figure 2. Because we are fitting to a distribution of points in a three-dimensional space, the fitting function will depend on two variables, and the natural choices are those that are distance independent, V and I_e. We want to minimize the fitting order, while still capturing the behavior of the distribution. As demonstrated by Zaritsky et al. (2006a) there is at least a second-order dependence on $\log \sigma$ and some dependence on $\log I_e$, and so we fit to second order in both $\log V$ and $\log I_e$ and include cross-terms. For this fit, we use only a randomly selected one-sixth of the Springob et al. (2007) sample to avoid having that sample dominate the fit. We present the coefficients of our fit in Table 1, but, because of the heterogeneous nature of the data and our avoidance of any type of Malmquist-like corrections (Willick 1994), these numbers are far from definitive.

The distinction between this work, with its complex characterization of Υ_e, and either FP or κ-space, with their assumption of homology, becomes evident when examining Figure 2. The projections of the data and the fitting function in Figure 2 illustrate that even in projection the functional form that describes Υ_e deviates from power laws. The top panels contain the inferred values of $\log \Upsilon_e - \text{const}$ from equation (5) versus either $\log V$ or $\log I_e$. The bottom panels, which show the fitted values, $\log \Upsilon_e^f$, and therefore have no intrinsic scatter, illustrate how the bulk of the observed scatter in the top panels comes simply from the projection of a complicated surface onto these axes. In other words, the reason galaxies of the same V have a range of Υ_e is not primarily because there is intrinsic scatter, say, due to age or metallicity, but rather because galaxies have a range of I_e. For a given V and I_e, the scatter in Υ_e is much smaller than that observed in Figure 2. To be specific, the scatter for the entire sample about the fit is 0.094 dex (24% rms in Υ_e). In contrast, the observed scatter in $\log \Upsilon_e$ in the top left panel of Figure 2 for $1.9 < V < 2$ is 0.22 dex (66% rms in Υ_e).

We are now ready to evaluate the degree to which equation (5) describes our set of galaxies. Replacing $\log \Upsilon_e - \text{const}$ with $\log \Upsilon_e^f$, we evaluate equation (5) and plot a rearrangement of the terms in Figure 3. By construction, equation (5) is satisfied on average when $\log \Upsilon_e - \text{const}$ is replaced by $\log \Upsilon_e^f$, which is evident in Figure 3. The actual test of our approach comes from examining the scatter about the mean and whether distinct galaxy populations fall off the mean trend. If galactic structure depends strongly on parameters not included in this simple description, then the scatter will be large. In other words, two galaxies that are identical in the quantities V, r_e, and I_e could, in principle, have very different values of Υ_e due to a dependence of Υ_e on accretion history, age, varying degrees of mass loss, or many other possible physical effects. These differences in Υ_e are not accounted for in Υ_e^f, thereby potentially leading to a large scatter about the mean. However, the scatter is only 0.094 for the entire sample. For reference, the scatter in this new relation for *all* galaxies is comparable to the scatter observed in either FP or TF studies for the relevant subset of galaxies. The scatter can be reduced slightly, to 0.084, if we correct each galaxy sample separately for zero-point shifts. These inferred zero-point shifts, obtained by calculating the mean offset relative to the 1:1 line, are all comparable to plausible photometric errors and generally correspond to a few hundredths of a magnitude (see Table 2).

The success of placing all galaxies onto a single surface in the (r_e, I_e, V) space demonstrates that, to within the scatter (<25%), the family of galaxies is a two-parameter sequence; i.e., measuring two of these structural parameters specifies the third. This implies that potentially important factors in galaxy development, such as environment, nuclear activity, star formation history, and accretion history, do not play a significant role in determining galactic structure *unless* they either move galaxies along the surface in (r_e, I_e, V) space or act in concert to preserve the manifold as the locus of equilibrium points of galactic structure. To reiterate, the important aspect of Figure 3 is not its linear nature, which is a result of our assertion that a fundamental manifold exists for all galaxies, but rather the low scatter and lack of any systematic departures for specific classes of galaxies, both of which imply that the assumptions that we have made so far are appropriate to this level of precision. In other words, random or systematic variations of A and B across either the mass range of galaxies or galaxy types, variations from isothermality, and any other factors that

[3] An alternate treatment that eventually leads to the same conclusion is to group together Υ_e, A, and B into a generic unknown, Δ, fit for Δ, and then use the argument in § 3.3 to demonstrate that $\Delta \propto \Upsilon_e$.

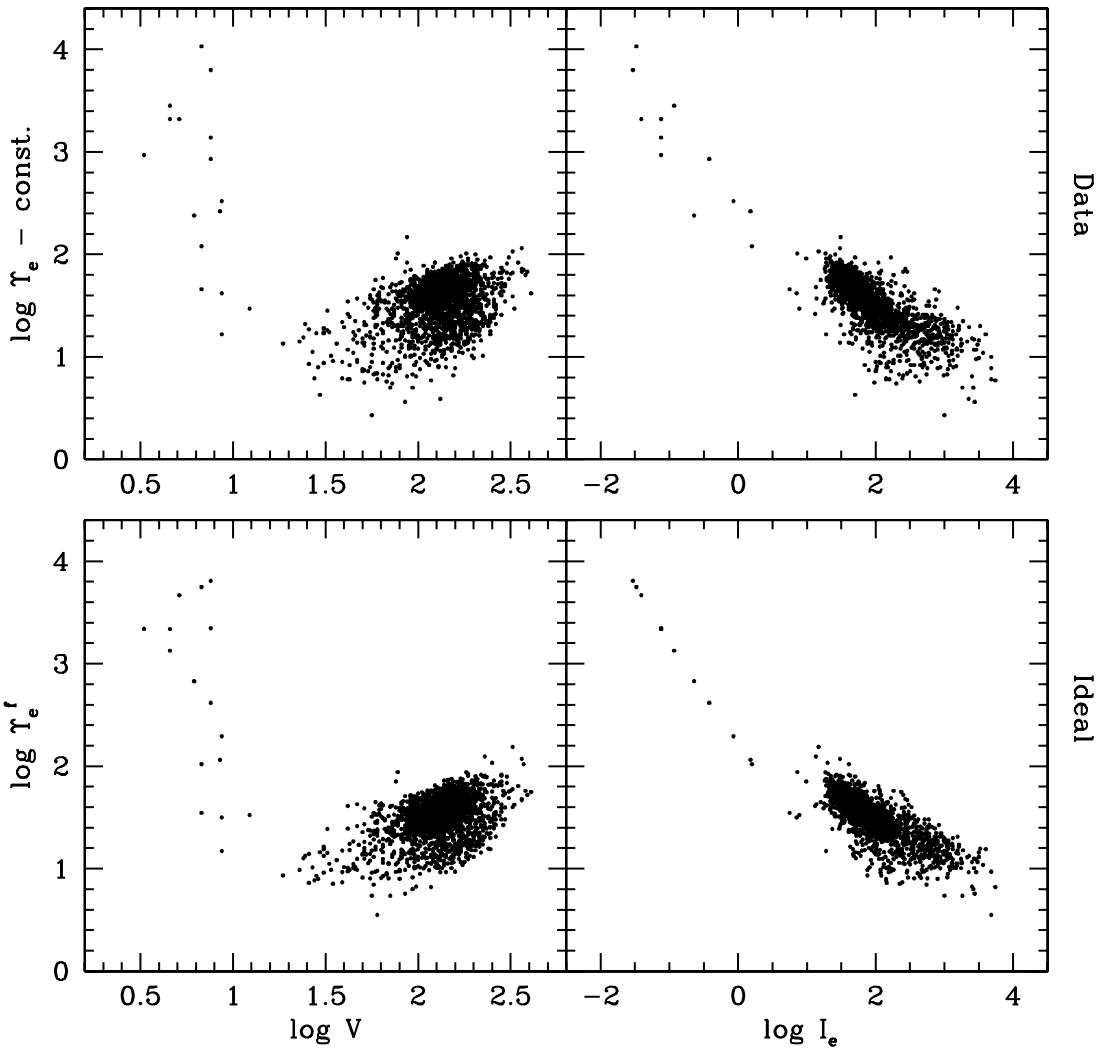

FIG. 2.—Projections of $\log \Upsilon_e$ and $\log \Upsilon_e^f$. *Top*: Plot of the projections of $\log \Upsilon_e$ − const, determined from eq. (5), vs. $\log V$ and $\log I_e$. *Bottom*: Plot of the values of $\log \Upsilon_e^f$ for every galaxy in our sample using the fit given in Table 1. The bottom panels illustrate that even with no intrinsic scatter in $\log \Upsilon_e^f$ the projections show significant apparent scatter. We conclude that the bulk of the apparent scatter in the top panels is due to the effects of projecting the complicated surface onto these axes, rather than to observational errors or intrinsic scatter.

are not considered contribute scatter that is at most the observed scatter, which is comparable to that measured in TF or FP studies.[4] We have achieved the first of the goals described in § 1 and now proceed to examine whether our attribution of the departures from homology to Υ_e is correct.

[4] Deconvolving the observational and random errors introduced by such real-world complications as projection effects, luminosity weighting of the kinematic measurements, and various biases from an "intrinsic" scatter is quite difficult, even for homogeneous samples (see Jørgensen et al. 1996; Springob et al. 2007), and beyond the scope of this study.

TABLE 1
Υ_e^f FIT COEFFICIENTS

Term	Coefficient
Constant	2.12
$\log V$	−0.01
$\log I_e$	−1.05
$\log^2 V$	0.07
$\log^2 I_e$	0.13
$\log V \log I_e$	0.14

3.3. *The Physical Validity of* Υ_e^f

The mathematical trick of placing all of the galaxy formation physics beyond the virial theorem into Υ_e potentially masks the importance of A and B. To check whether Υ_e^f truly reflects Υ_e or whether it is in actuality a composite of various terms, we compare Υ_e^f to independent determinations of Υ_e. We do this for both normal ellipticals and dSph's.

First, we compare to values of Υ_e derived from a full Schwarschild analysis of the two-dimensional line-of-sight velocity distributions, $\Upsilon_e^{\rm Sch}$, of normal elliptical galaxies (Cappellari et al. 2006, 2007). Because of the unknown constant in the definition of Υ_e^f relative to Υ_e, we have the freedom to normalize Υ_e^f to best match the Cappellari et al. (2006) data, which we do below (Fig. 4). Figure 4 illustrates the excellent correspondence between Υ_e^f and $\Upsilon_e^{\rm Sch}$. The agreement is particularly good (0.06 dex rms, 15% in Υ_e) for the galaxies that are most appropriate for our construction, namely, those in which the velocity dispersion dominates over systemic rotation and anisotropy measures are small ($|\beta, \gamma, \delta| < 0.15$ as measured by Cappellari et al. 2007). The scatter for those with large anisotropies is significantly greater (0.17 dex rms, 48% in Υ_e), suggesting that a full knowledge of A and B would decrease the scatter in Figure 3 among those

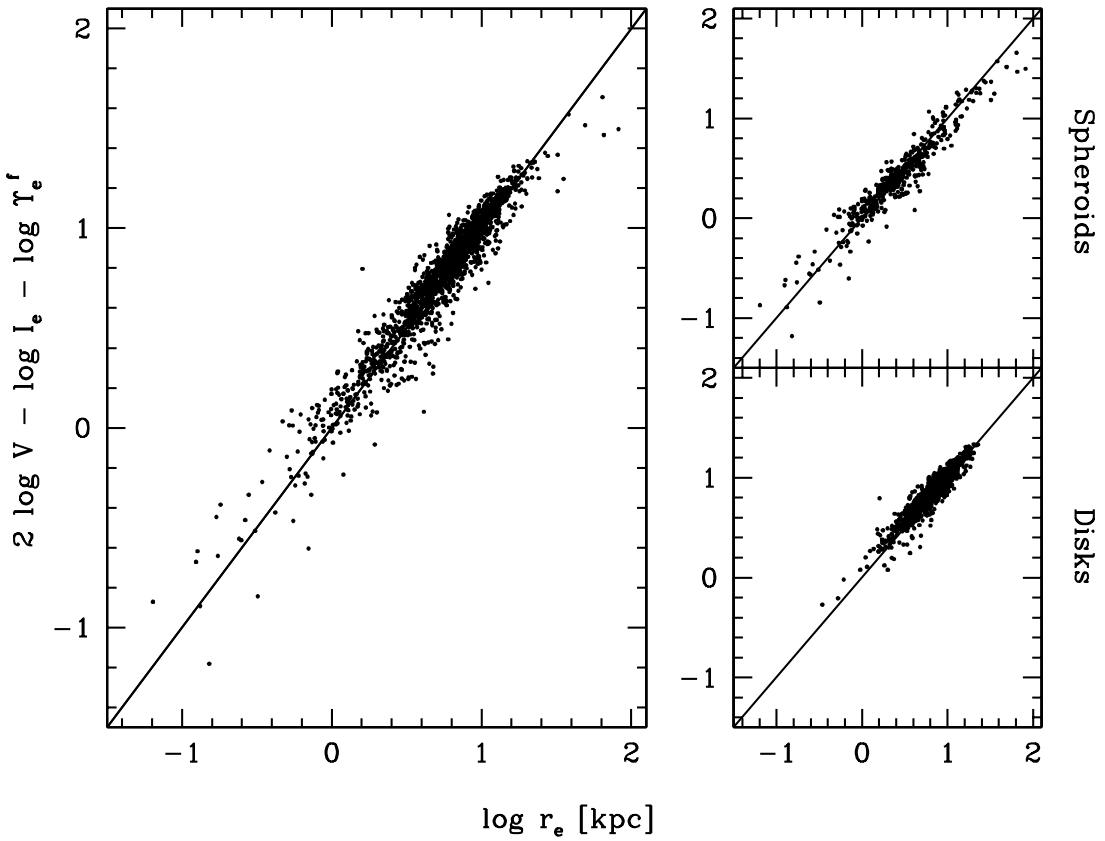

FIG. 3.—Testing an equation of galactic structure, eq. (5). We replace $\log \Upsilon_e$ − const with Υ_e^f to evaluate eq. (5) for the entire sample (*left*) and for spheroids and disks separately (*right*). By construction, the mean relation should lie along the 1:1 line. The low scatter and the lack of systematic deviations for galaxy subsamples testifies to the universal nature of this simple relation.

galaxies that do not fully satisfy the basic assumptions of our approach.

Second, we examine whether this correspondence holds across the range of galaxy masses. In Figure 4 we include values of $\log \Upsilon_e$ for Galactic dSph's estimated using Navarro-Frenk-White (NFW) model fits (Navarro et al. 1997) to the extensive kinematic data of Walker et al. (2007).[5] Unlike the Schwarschild analysis of normal elliptical galaxies, which has the freedom to include anisotropic velocity distributions, the Walker et al. (2007) analysis does not. The dSph data suggest a slightly different constant offset between $\log \Upsilon_e^f$ and $\log \Upsilon_e$ (-0.78 rather than -0.82), but this change is modest and has a nearly undetectable effect on the scaling relation when ignored (see Fig. 5). We adopt the average offset, -0.8, as the normalization constant and suggest an uncertainty in this number of ∼a few hundredths. Using this correspondence, we replace the constant in equation (5) to obtain

$$\log r_e - \log V^2 + \log I_e + \log \Upsilon_e + 0.8 = 0, \qquad (6)$$

where one can either evaluate Υ_e in some independent manner or express it in terms of V and I_e using the fit given in Table 1 and replacing $\log \Upsilon_e + 0.8$ with $\log \Upsilon_e^f$. Although this relationship was derived from I-band photometry, the only empirically derived quantity is the constant. Allowing for possible zero-point

[5] The calculated Υ_e use masses enclosed within r_e as calculated from the published fits, courtesy of Matthew Walker.

TABLE 2
RESULTS FOR INDIVIDUAL GALAXY SAMPLES IN FIGURE 3

Reference	N	Galaxy Types	Mean Offset	rms[a]
Oegerle & Hoessel (1991)	43	BCG	0.01	0.13 (0.13)
Jørgensen et al. (1996)	280	E/S0	−0.03	0.11 (0.10)
Geha et al. (2003)	17	dE	0.08	0.15 (0.12)
Matković & Guzmán (2005)	84	E/dE	−0.01	0.16 (0.16)
Various[b]	20	dE/dSph	0.05	0.23 (0.22)
Springob et al. (2007)	1319	S	0.04	0.07 (0.06)
Pizagno et al. (2007)	162	S	−0.04	0.10 (0.09)

[a] The quantity within parentheses represents the rms after correcting for the mean offset.
[b] The compilation of dSph data is described in Zaritsky et al. (2006a) and augmented with data from Simon & Geha (2007) and Walker et al. (2007).

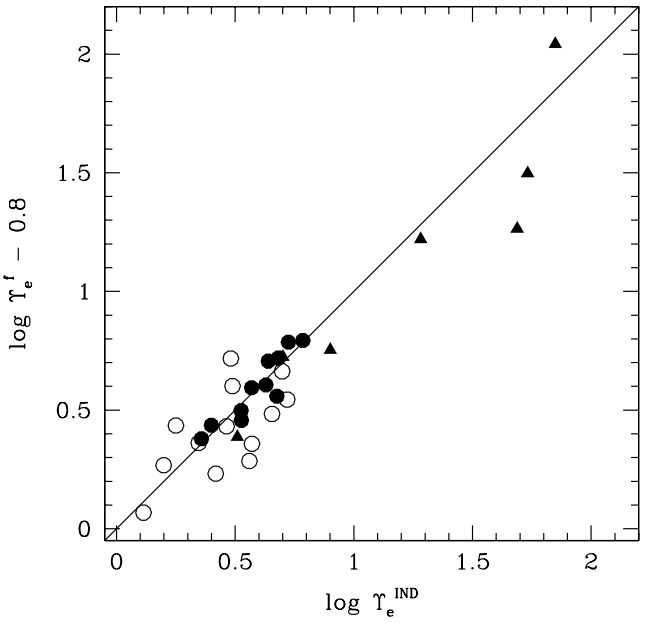

FIG. 4.—Comparison of mass-to-light ratios derived from independent means, Υ_e^{IND}, and our estimates of Υ_e using Υ_e^f. For normal elliptical galaxies (*circles*), we compare the mass-to-light ratio derived using the Schwarschild method of dynamical modeling for a set of nearby spheroidal galaxies (Cappellari et al. 2006) to our estimates of Υ_e using Υ_e^f. Open circles represent galaxies that Cappellari et al. (2006) note are fast rotators, and filled circles represent those that are not. The line is the 1:1 correspondence. The filled circles, which are the most appropriate comparison sample, show only 0.06 dex scatter (15% in Υ_e). For the Milky Way dSph galaxies (*triangles*), we compare the mass-to-light ratio derived from fitting NFW profiles to kinematic data (Walker et al. 2007) with our estimates of Υ_e using Υ_e^f. The unknown constant relating Υ_e^f to Υ_e is set to ensure agreement in the mean values of Υ_e^{IND} and Υ_e^f, and that value (−0.8) is then adopted for eq. (6).

offsets, we expect this relationship to hold at all wavelengths from which the stellar mass can be reliably estimated.

The applicability of the same normalization constant for both normal ellipticals and dSph's supports the contention that structural variations, as reflected by changes in A and B, are modest over most of the mass scale covered in Figure 3. Using these independently derived measures of Υ_e, we now return to equation (6), use the literature values for Υ_e rather than our fitting function, and plot the results in Figure 5. The difference between the left and right panels is the exclusion of the elliptical galaxies that show evidence for rotation or anisotropic velocity dispersions. The data in both panels follow the 1:1 correspondence well, although the correspondence in the right panel is striking. The scatter in that panel is 0.04 dex, or less than 10% in the parameter values themselves. We conclude that to a level of precision between 10% and 25% (the scatter measured using these independently measured values of Υ_e and the scatter measured using our fitting function, Υ_e^f, respectively), Υ_e encompasses all of the additional physics necessary to proceed from the virial theorem to a description of galactic structure. Thus, we achieve the second goal listed in § 1.

3.4. *Evolving onto the Manifold*

For various reasons, the small scatter seen in Figures 3 and 5 is remarkable. Even if r_e and V are the same in two similar galaxies, one might expect variations in the stellar mass-to-light ratios, Υ_*, of more than 50%, which would introduce scatter via variations in I_e. We suspect that at least part of the reason for the low observed scatter lies in the selection of galaxies in TF and FP studies, which generally favor evolved, dynamically relaxed galaxies, which are unlikely to exhibit dramatic variations in Υ_*. Therefore, we now return to the last of our disk galaxy samples (Geha et al. 2006), which contains disks with extremely high gas mass fractions and might therefore be expected to harbor systems with dramatically different values of Υ_* and Υ_e than those included in our analysis so far.

When the majority of the baryons in a galaxy are in the gas rather than in the stars, one might expect that our treatment as described above will fail because the connection between optical luminosity and mass via Υ_e becomes tenuous. In fact, the galaxies in the Geha et al. (2006) sample do fall off the surface, as shown in the top panel of Figure 6. However, as demonstrated with regard to the Tully-Fisher relation (McGaugh 2005; Geha et al. 2006), gas-rich and gas-poor galaxies have consistent scaling relationships if one considers total baryonic content instead of just that in the stellar component. Reviewing equations (2) and (3), it is evident that the derivation of later equations, such as equation (6), depended on a proxy for the enclosed mass. In light of previous studies, while optical luminosity may be an adequate proxy when most of the baryons are in the stars, it is clearly inadequate when the majority of baryons are in the gas (or, more precisely, our fitting formula for Υ_e fails when different fractions of the baryons are luminous in otherwise similar galaxies). The reason optical luminosity works well for most disks is that the majority of their cold gas has been turned into stars (Roberts 1969; Bothun 1984; Kannappan 2004; Read & Trentham 2005). Given that we do not have measured colors and gas masses for most of our sample, we cannot reformulate everything in terms of baryonic mass, but we can ask where these gas-rich galaxies would lie with respect to the 1:1 relationship in Figure 6 if they turned their gas into stars. Can they evolve onto the manifold?

To complete this exercise, we make two questionable assumptions. First, we assume that r_e does not change during the conversion of gas to stars. Because the gaseous and stellar radial distributions are likely to be different, this assumption must fail at some level. Second, we assume that the stellar population formed from the gas eventually has the same stellar mass-to-light ratio (i.e., for stars only) as the late-type galaxies in our sample ($\Upsilon_* = 0.97$ in the I band for a typical Sbc galaxy with $B - V = 0.57$; Fukugita et al. 1995; Bell & de Jong 2001). For these two assumptions, we then find the fraction of gas turned into stars that produces the best match to our scaling relation (eq. [6]). We exclude one galaxy with a rotational velocity of 5 km s^{-1}, which appears to be unphysically small, and one galaxy with $b/a > 0.9$, for which it is difficult to deproject the velocity width.

The result of this exercise, that these high gas mass fraction galaxies can evolve onto the relationship defined by the larger sample, is shown in the bottom panel of Figure 6. The resulting scatter is 0.16 dex, which is slightly lower than that found for the dSph's, but larger than for all of the galaxies combined. The difficulty with our scenario is that the agreement requires turning about 20% more gas than is available throughout the galaxy into stars. Perhaps this failure reflects the need for infalling gas, but it may also mean that as the galaxy evolves there is a corresponding change in r_e. For example, in a model in which the gas is funneled efficiently into the center so that r_e is only one-third of its current value and 75% of the current gas is turned into stars, the scatter about the relationship is only 0.14 dex. We conclude that there are plausible scenarios in which these gas-rich galaxies lie on the observed relationship and that one might identify galaxies that are still strongly evolving or those with a significant reservoir of cold gas as outliers from the manifold. Nevertheless, if either these galaxies convert their gas to stars or we properly account for their entire baryonic content within r_e, then we

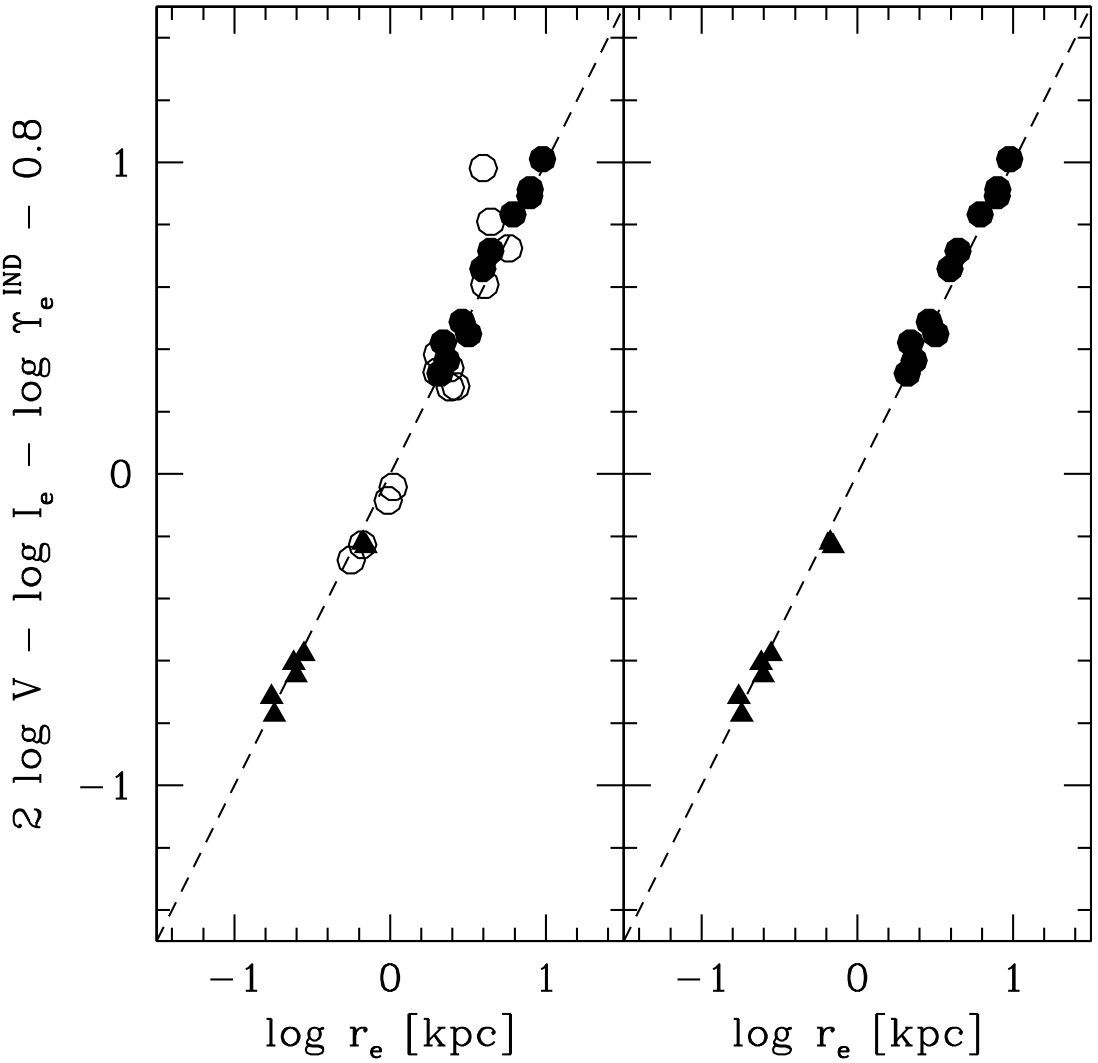

FIG. 5.—Scaling relationship, eq. (6), using $\Upsilon_e^{\rm IND}$ in place of Υ_e. Data and symbols are as in Fig. 4. *Left*: All of the spheroids with $\Upsilon_e^{\rm IND}$. The scatter is 0.09 dex about the 1:1 line, with a mean offset of 0.005. *Right*: Spheroids after removing the elliptical galaxies with either significant rotation or anisotropy (Cappellari et al. 2006, 2007). The scatter drops to 0.04 dex about the 1:1 line, with a mean offset of 0.004.

expect that they will satisfy the same scaling relation as all other galaxies.

3.5. *Revisiting Our Simplifications*

Before we proceed to discuss further implications of these results, we step back to explore how a failure to satisfy the assumptions invoked in our simplifications of the virial theorem would manifest itself in our evaluation of equation (6). The potential "failures" fall into three classes.

First, we might have introduced errors that are constant across the galaxy population. An example of such an error would be if we always underestimated the potential energy in our evaluation of the virial theorem by a fixed factor. Such an error would manifest itself as a zero-point shift of the data relative to the expectation. Because we do not calculate the specific constant in equation (6) from any physical argument, this type of error will be transparently absorbed into the constant term when we determine it using independent measurements, as done in § 3.3. For almost all of our discussion, this type of error is difficult to detect but irrelevant.

Second, we might have introduced errors that vary systematically across the galaxy population. An example of such an error would be if we underestimated the potential energy by a certain factor for low-mass systems, but overestimated it by a similar factor for high-mass systems. Such errors, to the degree that they correlate with at least one of the structural parameters, would lead to changes in the coefficients in equation (6) or that describe Υ_e^f (Table 1), but would not introduce scatter. This effect is analogous to introducing a tilt in FP analyses. Identifying this type of error is critical if one aims to understand the specific nature of the fitted relationships, such as that describing Υ_e^f, or to compare with simulations. We implicitly tested for such effects across galaxy types in § 3.2 and across galaxy mass in § 3.3. The coefficients derived from the virial theorem and a mass-to-light ratio that scales directly with independently derived mass-to-light ratios successfully produce a tight scaling relation (eq. [6]; Fig. 3). This result demonstrates that there is no effective tilt either with morphological type or across the full range of galaxy luminosities.

Third, we might have introduced errors that are variable and not systematic across the galaxy population. An example of such an error would be if we had ignored a key determining factor of galactic structure, e.g., the number of nearby neighbors. In naive models, close passages affect the luminosity of the system, but do not affect the size or internal kinematics, leading to potential outliers in equation (6). Such effects, to the degree that they do not correlate with the remaining structural parameters, will introduce

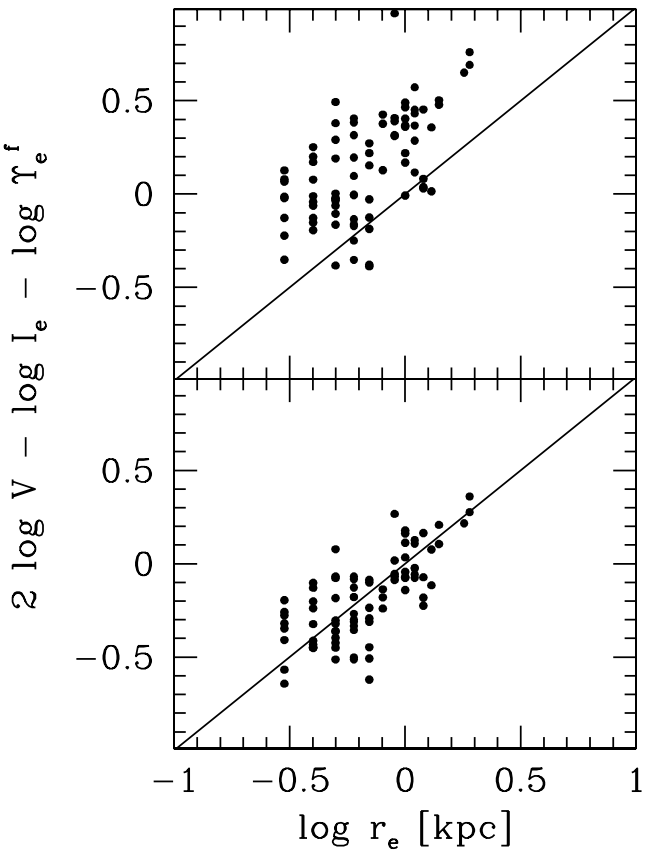

FIG. 6.—Results for the Geha et al. (2006) sample of disk galaxies with high gas mass fractions. *Top*: Galaxies (*points*) in comparison to the fitted relationship (*line*). *Bottom*: Where the galaxies might evolve as their gas is turned into stars.

scatter at each point in the (r_e, I_e, V) space. The low scatter in both the entire sample (Fig. 3) and the subsample with independently measured mass-to-light ratios (Fig. 5) demonstrates that any such errors introduce little noise.

3.6. *Connecting Υ_e to Physical Parameters*

What we have discussed so far are the end products, or observables (r_e, I_e, V, Υ_e), rather than inputs, or true physical quantities, that determine the structure of galaxies. Two natural candidates for the parameters that drive galactic structure are the mass and angular momentum of a galaxy. For disks, analytic treatments of galaxy formation using these two variables have been relatively successful (Fall & Efstathiou 1980; Dalcanton et al. 1997). Although these models require a few key assumptions that may not be entirely accurate, such as the conservation of angular momentum during collapse, their success, in combination with the results presented here, suggest that simple dynamical models may be able to reproduce the observable properties of galaxies. However, proceeding from such difficult-to-measure quantities as mass and angular momentum to the observed structure of galaxies in a single step is likely to prove difficult.

We focus instead on what we have learned so far from our analysis. Given that the virial theorem plus Υ_e are all one needs to generate a gross description of galactic structure (§§ 3.1–3.3), all of the interesting astrophysics of galaxy formation—at least as related to determining the current, gross structure of a galaxy—is encapsulated in Υ_e. What determines differences in Υ_e among galaxies?

First, galaxies might convert a different fraction, η, of their baryons to stars. Assuming a universal baryon–to–dark matter ratio for halos, this fraction can be measured using the total mass-to-light ratio, Υ_{200}, evaluated at R_{200}, the radius within which the mass density is 200 times the critical density and the system is roughly virialized. Systematic variations in η have already been noted in studies of halo occupation statistics (van den Bosch et al. 2003; Yang et al. 2005), lensing mass measurements (Hoekstra et al. 2005; Mandelbaum et al. 2006), and direct baryon measurements (Lin et al. 2004; Gonzalez et al. 2007). All of these studies show that Υ_{200}, and therefore η, depend on halo mass.

Second, the stars might be concentrated to varying degrees relative to the dark matter due to differences in the assembly history. We quantify the stellar concentration, ξ, using $\xi \equiv R_{200}/r_e$. As the stars become more concentrated in the halo, ξ increases and Υ_e decreases.

We now return to equation (2) with the aim of extracting from it expressions for the mass fraction of baryons that are converted to stars, η, and the degree to which the stars are concentrated relative to the dark matter, ξ. We rewrite equation (2) as appropriate at the virial radius, R_{200},

$$A_{200}V_{200}^2 = \frac{B_{200}GM_{200}}{R_{200}}, \tag{7}$$

where $M_{200} \equiv (4/3)\pi R_{200}^3 \rho_{200}$, $\rho_{200} \equiv 200\rho_{\rm crit}$, and $R_{200} \equiv \xi r_e$, where $\rho_{\rm crit}$ is the universal critical mass density at the present epoch. To make further progress, we set $V = V_{200}$. This is patently incorrect both because the dark matter potential itself is unlikely to be isothermal out to R_{200} (Navarro et al. 1997) and because any central concentration of the baryons will affect V. However, any constant fractional differences, for example, $V = 1.2V_{200}$ for all galaxies, will be absorbed later into our normalization. What do concern us, but are ignored here, are differences in this velocity scaling that depend on the properties of the galaxy (Courteau et al. 2007). This problem might be correctable in an iterative scheme (i.e., assume a nonisothermal potential, estimate ξ, evaluate the difference between V and V_{200}, correct V_{200}, and iterate until convergence) or in a more sophisticated model of galaxy formation (Somerville et al. 2008), but both of these remedies require some model assumptions and lead us away from the analytic descriptions that we aim to explore. Empirically, this problem might be addressed, at least for spiral galaxies, with the incorporation of radial information as is done in Tully-Fisher studies (Yegorova & Salucci 2007; Salucci et al. 2007). Work is needed to determine the magnitude of the error introduced by our simple treatment.

Continuing, we define η through the equation

$$L \equiv \frac{\eta f_B M_{200}}{\Upsilon_*}, \tag{8}$$

where Υ_* is the mass-to-light ratio of the stellar population, L is the total luminosity, and f_B is the baryon mass fraction. Algebra enables us to derive equations for ξ and η:

$$\xi = \left(\frac{3A_{200}}{800\pi\rho_{\rm crit}B_{200}G}\right)^{1/2}\frac{V}{r_e}, \tag{9}$$

$$\eta = \left(\frac{800\pi B_{200}^3 G^3 \rho_{\rm crit}}{3f_b^2 A_{200}^3}\right)^{1/2}\frac{L\Upsilon_*}{V^3}. \tag{10}$$

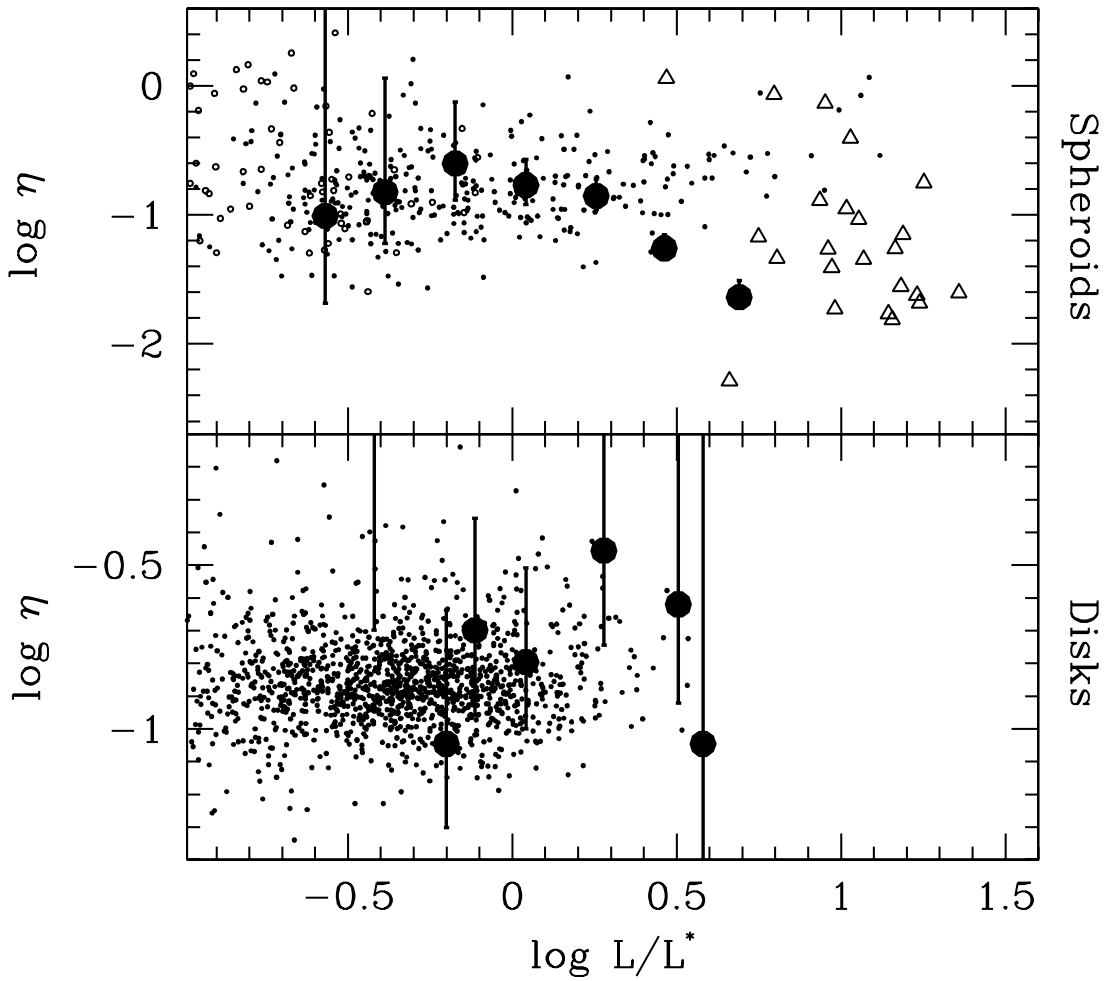

FIG. 7.—Fraction of baryons that are converted to stars, η, as a function of L/L^* for spheroids (*top*) and disks (*bottom*). Our data are shown as small dots. The values from Mandelbaum et al. (2006) are shown as large filled circles with error bars and represent average values for bins of L/L^*. This plot includes the cluster spheroids of Zaritsky et al. (2006a; *triangles*), so that we extend the range of L/L^* to the higher luminosities (see text) probed by Mandelbaum et al. (2006).

We express the combination of these two quantities as

$$\log \xi + \log \eta = \log \frac{KV}{r_e} + \log \frac{JL\Upsilon_*}{V^3}, \tag{11}$$

where all constants, as well as the structural factors A_{200} and B_{200}, in equations (9) and (10) are contained in K and J. A_{200} and B_{200} are not necessarily constant, although their analogs at r_e are well behaved (§ 3.2). We assume that A_{200} and B_{200} are similarly well behaved at R_{200}. Rewriting, we get

$$\log \xi + \log \eta = -2 \log V + \log r_e + \log I_e + \log \Upsilon_* + \text{const.} \tag{12}$$

We know from § 3.2 that we can replace the three leading terms on the right-hand side with $-\log \Upsilon_e$ to within a constant, so

$$\log \xi + \log \eta = -\log \Upsilon_e + \log \Upsilon_* + \text{const.} \tag{13}$$

Because $\Upsilon_e = f(V, I_e)$, as defined in Table 1, $\log \eta + \log \xi$ is also a function of V and I_e.

To provide a more direct example of the possible use of these equations, we use the results from Mandelbaum et al. (2006) to evaluate the constant terms (including the assumed constant terms A_{200} and B_{200}) in equations (9) and (10). Mandelbaum et al. (2006) use results from weak lensing to evaluate the fraction of baryons that are turned into stars as a function of galaxy luminosity. They provide empirical values for η as a function of galaxy luminosity and morphology. We use their results for η for L^* spiral galaxies and assume $\Upsilon_* = 1.7$ in the I band and a universal baryon mass fraction of 0.175 (Spergel et al. 2007) to set the values of the leading coefficients in our equations (9) and (10), $\xi = 1.4Vr_e^{-1}$ and $\eta = 1.9 \times 10^{-5}(L/L^*)\Upsilon_* V^{-3}$, respectively. The adopted value of Υ_* for an L^* spiral galaxy (assuming that it is an Sab type with $B - V = 0.8$; Fukugita et al. 1995) is calculated using Table 1 of Bell & de Jong (2001). We then plot our calculated values of η for all of our galaxies (Fig. 7), assuming that Υ_* is 1.7 and 2.5 for disks and spheroids, respectively. For the purpose of this comparison, we augment our galaxy sample with measurements of cluster spheroids (CSph's), the brightest cluster galaxy plus the intracluster stars of groups and clusters (Zaritsky et al. 2006a). Our previous work shows that these systems lie on the FM and, in this context, they allow us to extend the range of L/L^* over which we can compare to the Mandelbaum et al. (2006) results. We decided against including the CSph's throughout our current study because our focus is on galaxies, but CSph's do indeed fall on the 1:1 line in Figure 3.

Our values for η are in agreement over the range of luminosities and galaxy types presented by Mandelbaum et al. (2006), except possibly for the highest luminosity spheroids: brightest cluster galaxies and CSph's. Our data suggest a drop in η qualitatively similar to that found by Mandelbaum et al. (2006), although

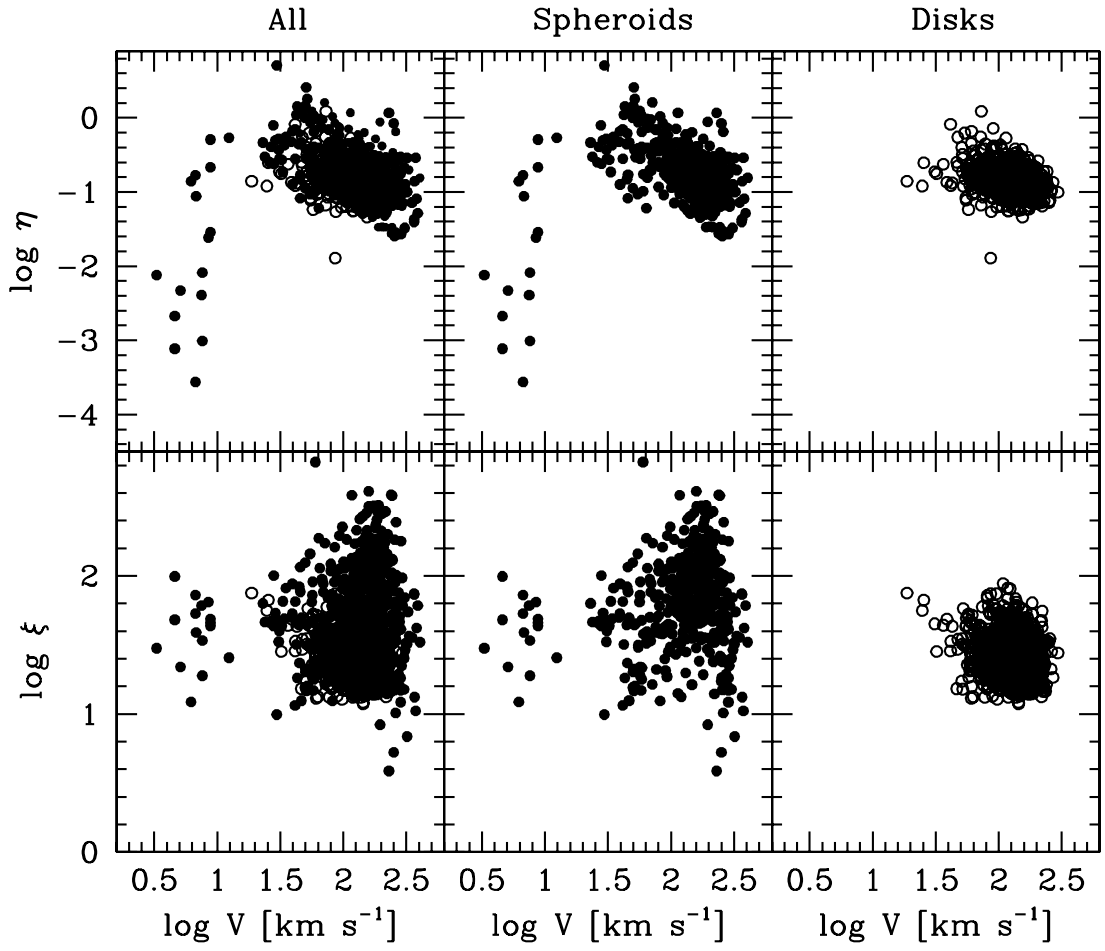

FIG. 8.—Mass fraction of baryons that are converted to stars, η (*top*), and stellar concentration, ξ (*bottom*), as a function of V for our entire sample (spheroids represented by fil led circles, disks by open circles). Various results are in evidence, including the dramatic decrease in η for the dSph's, the similarity in η among spiral galaxies and spheroids in the regime where they overlap in V, the systemic decline in η with increasing V for $\log V > 1.5$, and the generally greater ξ for spheroids relative to disks in that same velocity range.

at somewhat larger values of L/L^*. There are many technical reasons (such as the use of different bandpasses, subtleties in the definition of total magnitudes, and complications introduced by intracluster light for these most massive spheroids) that preclude any conclusion about whether there is a true discrepancy. In general, we agree quite well both qualitatively and quantitatively with their results. This agreement, in turn, suggests that A_{200} and B_{200} do not vary strongly as a function of mass or morphological type.

We proceed now to calculate η and ξ as a function of V for all of our galaxies and show the results in Figure 8. Here, to within the limitations of our simple derivation and the heterogeneous sample, is a full description of how baryons turn into stars and distribute themselves in all galaxies ranging from dSph's to brightest cluster galaxies (BCGs). There are several striking results. First, the relatively large values of Υ_e for dwarf spheroidals are primarily driven by η rather than by ξ, which is surprisingly constant across the full range of V. Second, at a given V, elliptical and spiral galaxies have similar values of η. Therefore, the differences in their values of Υ_e are due primarily to differences in ξ. Third, there is a steady decline in η for $\log V > 1.5$ ($V > 32$ km s^{-1}), even for the spheroids, among which large variations in Υ_* are less likely. Systems with V comparable to the Milky Way, 149 km s$^{-1} < V < 163$ km s^{-1} or, alternatively, 210 km s$^{-1} < v_c < 230$ km s^{-1}, have $\eta = 0.14 \pm 0.04$, with the spheroids being on average 5 times more concentrated than the disks. All of these results await resolution of two key open questions in the evaluation of ξ and η: (1) how to treat the difference between V and V_{200} and (2) whether the structural terms are as well behaved at R_{200} as they are at r_e. Nevertheless, this analysis illustrates how we might construct a bridge between the empirical relations based on observables and more theoretical ones based on fundamental physical parameters. Thus, we achieve the third goal listed in § 1.

4. SUMMARY

We have shown that all classes of galaxies, ranging in mass from dwarf spheroidals to brightest cluster galaxies and in type from spheroids to disks, fall on a two-dimensional surface in the observable space (r_e, I_e, V), where $V^2 \equiv (1/2)v_c^2 + \sigma^2$, over 3 orders of magnitude in r_e, with <25% scatter. The scatter about that surface is comparable to that observed in fundamental plane and Tully-Fisher studies in which the range of galaxy types and luminosities is much more limited. The TF and FP relationships are subsets of the manifold presented here. This finding alone demonstrates that the structure of all galaxies can be described with a highly limited set of parameters. The observational ones (r_e, I_e, and V) may not be optimal, even though they do a remarkably good job. The small scatter about the mean relation implies that a host of potential physical phenomena, such as environmental effects, star formation history, nuclear activity, accretion history, and feedback, either (1) are relatively unimportant in determining the structure of galaxies, (2) move galaxies along this

well-defined relationship, or (3) balance each other so as to define the mean relation as the locus of galactic structure equilibria.

We developed a simple analytic treatment in which we asserted the existence of a fundamental manifold of galaxies. By requiring the simple virial theorem derivation to result in a two-dimensional manifold in observed space, we specify the behavior of the mass-to-light ratio within r_e, and Υ_e. We then tested this assertion by comparing our inferred values of Υ_e to those derived independently from much more sophisticated modeling for both normal ellipticals and dSph's. The agreement is quantitatively excellent, with less than 15% scatter in mass-to-light ratios for those galaxies that satisfy our dynamical criteria. This result demonstrates that the principal additional ingredient necessary to proceed from the virial theorem to a description of galactic structure is knowledge of the mass-to-light ratio within r_e. Additional factors that could have been important, such as internal kinematic anisotropy or variations in the radial profile of the gravitational potential from one galaxy to another, must play a role at less than the 25% level. The observed manifold is described by

$$\log r_e - \log V^2 + \log I_e + \log \Upsilon_e + 0.8 = 0, \qquad (14)$$

where we also provide a fitting function for $\log \Upsilon_e$ in terms of V and I_e. The equations presented here are numerically appropriate for r_e, I_e, and V, and Υ in units of kpc, km s^{-1}, $L_\odot$ pc^{-2}, and solar units, respectively, and are based primarily on I-band observations.

We then discuss what the inferred behavior of Υ_e may mean for the physical characteristics of the galaxies. In particular, we speculate that the two principal determinants of Υ_e are the mass fraction of baryons that are turned into stars, η, and the degree to which the stars are spatially concentrated relative to the dark matter, $\xi \equiv R_{200}/r_e$. We derive equations for both quantities in terms of unknown structural parameters and the observables. We relate the two quantities using the expression that we derived for Υ_e. Finally, we use independent measures of η (Mandelbaum et al. 2006) to solve for the unknown structural terms for one set of galaxies and then compare the behavior of η across other luminosities and galaxy types as determined both from our analysis and that independent weak-lensing study. This comparison leads to simple expressions for η and ξ,

$$\eta = 1.9 \times 10^{-5} \frac{(L/L^*)\Upsilon_*}{V^3}, \qquad (15)$$

$$\xi = 1.4 \frac{V}{r_e}. \qquad (16)$$

We are then able to extend the measurements of η and ξ to the full range of galaxies. As rough guides, we find that, for most galaxies, $0.04 < \eta < 0.6$ and $10 < \xi < 200$, although these can be evaluated on a galaxy-by-galaxy basis. Systems with V comparable to the Milky Way, 149 km s^{-1} $< V <$ 163 km s^{-1} or, alternatively, 210 km s^{-1} $< v_c <$ 230 km s^{-1}, have $\eta = 0.14 \pm 0.04$, with the spheroids being on average 5 times more concentrated than the disks. Overall, we reach a set of general conclusions. First, the relatively large values of Υ_e for dwarf spheroidals are primarily driven by η rather than by ξ, which is surprisingly constant across the full range of V. Second, at a given V, elliptical and spiral galaxies have similar values of η (<10% difference for spheroids and disks with 149 km s^{-1} $< V <$ 163 km s^{-1}). Therefore, the difference in their values of Υ_e is due primarily to differences in ξ. Third, there is a steady decline in η for $\log V > 1.5$ ($V > 32$ km s^{-1}).

These results apply to the vast majority of galaxies, but not necessarily to all galaxies. In particular, we use a galaxy's luminosity as a proxy for its baryonic mass, and therefore, galaxies that have the bulk of their baryons in nonstellar components will not fit the relations as formulated (see § 3.4). Alternative formulations that account for the baryonic mass in other ways, analogously to what has been done to produce the baryonic TF relation (McGaugh et al. 2000), might be even more general that what we provide here.

The data used here fall short of the ideal sample from which to properly derive the quantitative values that mathematically describe the manifold, primarily due to the heterogeneous nature of the amalgamated sample. Nevertheless, the combined sample does demonstrate that the range of galaxy structure is dominated by only two parameters and that differences in sample selection or measurements among samples are not statistically discernible. The lower scatter obtained either for a single sample (0.06 dex for the Springob et al. [2007] disk sample) or for independently derived Υ_e (0.04 dex when using both the Cappellari et al. [2006] data for elliptical galaxies and the Walker et al. [2007] data for dSph's) suggests that a homogeneous sample might show that the myriad of possible influences on galactic structure (environment, accretion history, an active galactic nucleus, star formation history, and others) contribute at most a $\sim$10% scatter to the scaling relationship presented in equation (14).

The existence of a highly constrained surface on which galaxies lie does not eliminate the need for additional physics. In particular, as we have hinted throughout, many physical effects might move galaxies along the surface or perhaps counterbalance to move galaxies back to the equilibrium surface described by the manifold. As such, future galaxy models may be more constrained by the distribution of galaxies on the surface rather than perpendicular to it. Our heterogeneous sample is ill suited to say much about the distribution of sources on the surface. Much work still remains.

We close by returning to the analogy of stellar structure. It is evident that we are still far from a physical theory of galactic structure, but we have progressed in several key aspects. First, we have now demonstrated that the entire family of galaxies can be described by sets of two parameters (e.g., V and I_e, or η and ξ). This finding motivates the search for relatively simple expressions of galactic structure that are connected to a small set of physical parameters, such as mass and angular momentum. Second, we have identified the principal characteristic that remains to be explained, namely, Υ_e. The virial theorem plus an understanding of Υ_e are all that are necessary to predict the size, internal kinematics, or luminosity of a galaxy when given the other two. This in turn places the focus on understanding what determines the fraction of baryons that are turned into stars and how those stars are packed within the dark halo. If those quantities can then be connected to more fundamental parameters, such as mass and angular momentum, then one could proceed from the physical parameters directly to the observables. At that point, we will have indeed produced equations of galactic structure.

D. Z. acknowledges financial support for this work from a Guggenheim fellowship, NASA LTSA award NNG05GE82G, and NSF grant AST 03-07482. A. I. Z. acknowledges financial support from NASA awards LTSA NAG5-11108 and ADP NNG05GC94G, and from NSF grant AST 02-06084. D. Z. and A. I. Z. also want to thank the NYU Physics Department and the Center for Cosmology and Particle Physics for their generous support and hospitality during their sabbatical there.

REFERENCES

Bell, E. F., & de Jong, R. S. 2001, ApJ, 550, 212
Bernardi, M., et al. 2003, AJ, 125, 1866
Bothun, G. D. 1984, ApJ, 277, 532
Burstein, D., Bender, R., Faber, S., & Nolthenius, R. 1997, AJ, 114, 1365
Cappellari, M., et al. 2006, MNRAS, 366, 1126
———. 2007, MNRAS, 379, 418
Courteau, S., McDonald, M., Widrow, L. M., & Holtzman, J. 2007, ApJ, 655, L21
Dalcanton, J. J., Spergel, D. N., & Summers, F. J. 1997, ApJ, 482, 659
Djorgovski, S., & Davis, M. 1987, ApJ, 313, 59
Dressler, A., Lynden-Bell, D., Burstein, D., Davies, R. L., Faber, S. M., Terlevich, R., & Wegner, G. 1987, ApJ, 313, 42
Faber, S. M., & Gallagher, J. S. 1979, ARA&A, 17, 135
Faber, S. M., & Jackson, R. E. 1976, ApJ, 204, 668
Fall, S. M., & Efstathiou, G. 1980, MNRAS, 193, 189
Fukugita, M., Shimasaku, K., & Ichikawa, T. 1995, PASP, 107, 945
Gavazzi, R., Treu, T., Rhodes, J. D., Koopmans, L. V. E., Bolton, A. S., Burles, S., Massey, R. J., & Moustakas, L. A. 2007, ApJ, 667, 176
Geha, M., Blanton, M. R., Masjedi, M., & West, A. A. 2006, ApJ, 653, 240
Geha, M., Guhathakurta, P., & van der Marel, R. P. 2003, AJ, 126, 1794
Gonzalez, A. H., Zaritsky, D., & Zabludoff, A. I. 2007, ApJ, 666, 147
Hoekstra, H., Hsieh, B. C., Yee, H. K. C., Lin, H., & Gladders, M. D. 2005, ApJ, 635, 73
Jørgensen, I., Franx, M., & Kjaergaard, P. 1996, MNRAS, 280, 167
Kannappan, S. J. 2004, ApJ, 611, L89
Kassin, S. A., et al. 2007, ApJ, 660, L35
Lin, Y.-T., Mohr, J. J., & Stanford, S. A. 2004, ApJ, 610, 745
Mandelbaum, R., Seljak, U., Kauffmann, G., Hirata, C. M., & Brinkmann, J. 2006, MNRAS, 368, 715
Matković, A., & Guzmán, R. 2005, MNRAS, 362, 289
McGaugh, S. S. 2005, ApJ, 632, 859
McGaugh, S. S., Schombert, J. M., Bothun, G. D., & de Blok, W. J. G. 2000, ApJ, 533, L99
Navarro, J. F., Frenk, C. S., & White, S. D. M. 1997, ApJ, 490, 493
Oegerle, W. R., & Hoessel, J. G. 1991, ApJ, 375, 150
Pizagno, J., et al. 2007, AJ, 134, 945
Read, J. I., & Trentham, N. 2005, Philos. Trans. R. Soc. London, A, 363, 2693
Roberts, M. S. 1969, AJ, 74, 859
Salucci, P., Lapi, A., Tonini, C., Gentile, G., Yegorova, I., & Klein, U. 2007, MNRAS, 378, 41
Simon, J. D., & Geha, M. 2007, ApJ, 670, 313
Somerville, R., et al. 2008, ApJ, 672, 776
Spergel, D. N., et al. 2007, ApJS, 170, 377
Springob, C. M., Masters, K. L., Haynes, M. P., Giovanelli, R., & Marinoni, C. 2007, ApJS, 172, 599
Tully, R. B., & Fisher, J. R. 1977, A&A, 54, 661
van den Bosch, F. C., Yang, X., & Mo, H. J. 2003, MNRAS, 340, 771
Walker, M. G., Mateor, M., Olszewski, E. W., Gnedin, O. Y., Wang, X., Sen, B., & Woodroofe, M. 2007, ApJ, 667, L53
Willick, J. A. 1994, ApJS, 92, 1
Yang, X., Mo, H. J., Jing, Y. P., & van den Bosch, F. C. 2005, MNRAS, 358, 217
Yegorova, I. A., & Salucci, P. 2007, MNRAS, 377, 507
Zaritsky, D., Gonzalez, A. H., & Zabludoff, A. I. 2006a, ApJ, 638, 725
———. 2006b, ApJ, 642, L37